Genuinely Upwind Algorithms for the Multidimensional Euler Equations

C. Lacor* and Ch. Hirsch*
Vrije Universiteit Brussel, Brussels, Belgium

A new method for the solution of the multidimensional Euler equations is presented. As opposed to the classical schemes, it is genuinely multidimensional in that the local characteristic directions, into which information is propagated, are detected. Based on this approach, a conservative cell-centered scheme has been formulated. The numerical fluxes are evaluated using MUSCL extrapolations along the characteristic directions. This leads to a family of first- and second-order accurate schemes with an improved resolution as compared to the classical schemes.

Introduction

CLASSICAL upwind schemes for the Euler equations can roughly be divided into two categories: flux vector splitting type schemes and Godunov type schemes.

In flux vector splitting type schemes,[1,2] an upwind discretization is obtained by splitting the flux vector into two parts that are based on information respectively upwind and downwind of the cell face. The splitting is based on a locally one-dimensional investigation of the eigenvalues of the Euler system.

The Godunov type schemes[3-5] consist of a projection stage and an evolution stage. The projection stage determines the spatial accuracy of the scheme. The initial solution is redistributed using interpolation so that it is continuous within each cell. In the evolution stage, the solution is updated to the new time level by locally solving the Riemann problem on the cell faces. In the original Godunov scheme,[3] the local Riemann problem is solved exactly. Roe[4] and Osher and Solomon[5] instead use approximate Riemann solvers.

All of these schemes were originally developed for the one-dimensional Euler equations and are therefore based on one-dimensional theory. The extension into multidimensions is obtained by straightforward extrapolation of the one-dimensional ideas: in each grid direction the problem is treated as if it was one dimensional. This introduces a nonphysical grid dependency that leads to a reduced accuracy.

Recently, some new ideas have been formulated for the definition of genuinely multidimensional Euler schemes.[6-8]

Roe[6] decomposes a two-dimensional flow variation into eight simple waves that propagate into specific directions determined from certain combinations of velocity gradients. Each of these wave amplitudes is further discretized in an upwind way in accordance to the associated wave speed.

Hirsch[7] and Deconinck et al.[8] propose a local diagonalization of the Euler system based on two characteristic directions, depending on the local flow gradients. If no diagonalization is possible the directions are chosen as to minimize off-diagonal terms.

Hirsch et al.[9] formulate a two-dimensional explicit, nonconservative scheme based on these ideas. Powell and van Leer[10] develop a genuinely two-dimensional extension of Roe's cell-vertex scheme,[4] thereby using the characteristic directions as formulated in Refs. 7 and 8. The schemes developed in Refs. 9 and 10 both show an improved resolution as compared to the classical upwind schemes.

The present paper is a sequel to Ref. 9 and proposes a conservative, cell-centered, implicit scheme. The expression for the numerical fluxes is similar to that of Roe's flux-differencing scheme,[11] but is based on the characteristic directions instead of the cell normals. To fully exploit the information given by the local diagonalization, the new scheme is combined with a MUSCL extrapolation into the characteristic directions.

Diagonalization of the Multidimensional Euler Equations

The theoretical framework, given in Refs. 8 and 9, is shortly repeated hereunder. The two-dimensional Euler equations can be written as

$$\frac{\partial U}{\partial t} + \frac{\partial F}{\partial x} + \frac{\partial G}{\partial y} = 0 \tag{1}$$

where U is the vector of conservative variables and F,G represent the flux vectors. The quasilinear form of Eq. (1) is

$$\frac{\partial U}{\partial t} + A\frac{\partial U}{\partial x} + B\frac{\partial U}{\partial y} = 0 \tag{2}$$

where A and B are the Jacobian matrices.

In two- or three-dimensional Euler flows, information is propagated in infinitely many directions, each one corresponding to an arbitrary wave front normal, denoted κ. For

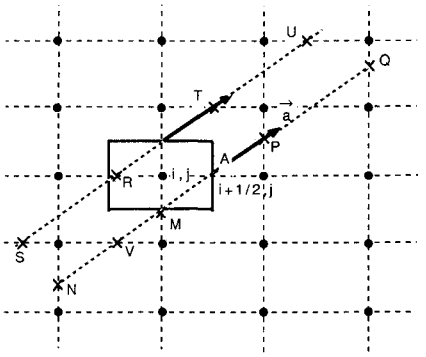

Fig. 1 MUSCL extrapolation along a characteristic direction.

Presented as Paper 89-1958 at the AIAA 9th Computational Fluid Dynamics Conference, Buffalo, NY, June 14-16, 1989; received Aug. 30, 1989; revision received March 2, 1991; accepted for publication March 6, 1991.

*Professor, Department of Fluid Mechanics. Member AIAA.

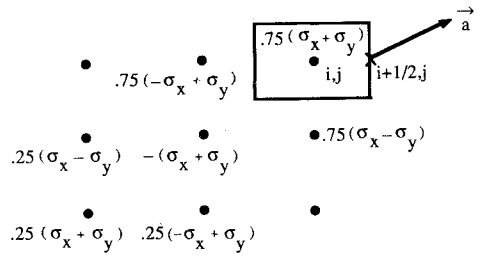

Fig. 2 Molecule for second-order accurate characteristic MUSCL applied to scalar, linear convection.

any choice of κ, a similarity transformation can be defined that diagonalizes $A \cdot \kappa$ with $A = (A,B)$:

$$A \cdot \kappa = P\, D\, P^{-1} \tag{3}$$

where D is a diagonal matrix containing the characteristic speeds of propagation associated with κ. Introducing characteristic variables $\partial \tilde{W}$,

$$\partial \tilde{W} = P^{-1}\, \partial U \tag{4}$$

the Euler equations are recast into the following form:

$$\frac{\partial \tilde{W}}{\partial t} + P^{-1} A P \frac{\partial \tilde{W}}{\partial x} + P^{-1} B P \frac{\partial \tilde{W}}{\partial y} = 0 \tag{5}$$

Since the Jacobian matrices do not commute the Euler equations are not diagonalized.

However, in Refs. 8 and 9, two different directions κ_1 and κ_2 were chosen locally. The transformation matrices are now denoted with an asterisk superscript. New characteristic variables ∂W can now be defined:

$$\partial W = P^{*-1}\, \partial U \tag{6}$$

where the transformation matrix P^* is given by

$$P^* = \begin{bmatrix} 1 & 0 & \frac{\rho}{2c} & \frac{\rho}{2c} \\ u & \rho\frac{\kappa_{2y}}{K} & \frac{\rho}{2cK}(uK + c\kappa_{1x}) & \frac{\rho}{2cK}(uK - c\kappa_{1x}) \\ v & -\rho\frac{\kappa_{2x}}{K} & \frac{\rho}{2cK}(vK + c\kappa_{1y}) & \frac{\rho}{2cK}(vK - c\kappa_{1y}) \\ \frac{v^2}{2} & \frac{\rho}{K}(u\kappa_{2y} - v\kappa_{2x}) & \frac{\rho}{2cK}(HK + cv\kappa_1) & \frac{\rho}{2cK}(HK - cv\kappa_1) \end{bmatrix} \tag{7}$$

where H is the total enthalpy, K the dot product of the two characteristic directions, and the subscripts x,y denote x and y components of vectors. The expression for P^{*-1} is given in Ref. 9 and will not be repeated here. The following expressions for the characteristic variables result:

$$\partial W = \begin{bmatrix} \partial w^1 \\ \partial w^2 \\ \partial w^3 \\ \partial w^4 \end{bmatrix} = \begin{bmatrix} \partial\rho - \frac{1}{c^2}\partial p \\ \kappa_{1y}\partial u - \kappa_{1x}\partial v \\ \kappa_2 \cdot \partial v + \frac{\partial p}{\rho c} \\ -\kappa_2 \cdot \partial v + \frac{\partial p}{\rho c} \end{bmatrix} \tag{8}$$

The Euler system Eq. (1) is then equivalent to

$$\frac{\partial W}{\partial t} + (\Lambda_x + C_x)\frac{\partial W}{\partial x} + (\Lambda_y + C_y)\frac{\partial W}{\partial y} = 0 \tag{9}$$

where

$$P^{*-1} A P^* = \Lambda_x + C_x \tag{10}$$

$$P^{*-1} B P^* = \Lambda_y + C_y \tag{11}$$

The diagonal matrices are given by

$$\Lambda_x = \begin{bmatrix} u & \cdot & \cdot & \cdot \\ \cdot & u & \cdot & \cdot \\ \cdot & \cdot & u + c\kappa_{2x} & \cdot \\ \cdot & \cdot & \cdot & u - c\kappa_{2x} \end{bmatrix} \tag{12a}$$

$$\Lambda_y = \begin{bmatrix} v & \cdot & \cdot & \cdot \\ \cdot & v & \cdot & \cdot \\ \cdot & \cdot & v + c\kappa_{2y} & \cdot \\ \cdot & \cdot & \cdot & v - c\kappa_{2y} \end{bmatrix} \tag{12b}$$

The system, Eq. (9), is diagonalized if the coupling terms vanish, i.e., if

$$C_x \frac{\partial W}{\partial x} + C_y \frac{\partial W}{\partial y} = 0 \tag{13}$$

One can show that this leads to the following constraints on the local directions κ_1 and κ_2:

$$\kappa_1 \times \nabla p = 0 \tag{14}$$

$$\kappa_2(\kappa_2 \cdot \nabla)v - \nabla \cdot v = 0 \tag{15}$$

Equations (14) and (15) relate the characteristic directions to the local gradients of the flow variables.

Equation (14) is easily satisfied analytically. In uniform flow, the pressure gradient vanishes and κ_1 is arbitrary. In the code, κ_1 is chosen into the velocity direction for small pressure gradients. This may locally cause a switch into the direction of κ_1 if the pressure gradient varies from one iteration to another. This can be avoided by choosing the first characteristic direction as a blending of the velocity direction and the direction of pressure gradient, as used by Levy et al.[12]

Equation (15) cannot always be fulfilled. In Ref. 8, it is shown that it can be satisfied if the principal strain rates, denoted ε_X, ε_Y, have opposite signs. In this case, two solutions for κ_2 exist. κ_2 is then chosen in order to maximize the scalar product $\kappa_1 \cdot \kappa_2$ in absolute value. This corresponds to the maximization of $\det [P^{*-1}]$ which is proportional to $\kappa_1 \cdot \kappa_2$. If Eq. (15) has no solution, no complete diagonalization of the system, Eq. (9), is possible. To minimize the off-diagonal terms, κ_2 is then chosen to minimize the left-hand side of Eq. (15).

Once the characteristic directions are found, several numerical schemes can be defined.

A nonconservative numerical scheme, already suggested in Ref. 9, consists of discretizing the scalar equations with an explicit, upwind scheme, with eventual coupling terms treated as source terms. The update for the characteristic variables ∂W is transformed into a correction for the conservative variables using Eq. (6).

Two different upwind schemes were tested: the classical first-order upwind scheme and a first-order streamline upwind scheme, with significantly less numerical diffusion, corresponding to a linear version of a scheme proposed by Rice and Schnipke.[13]

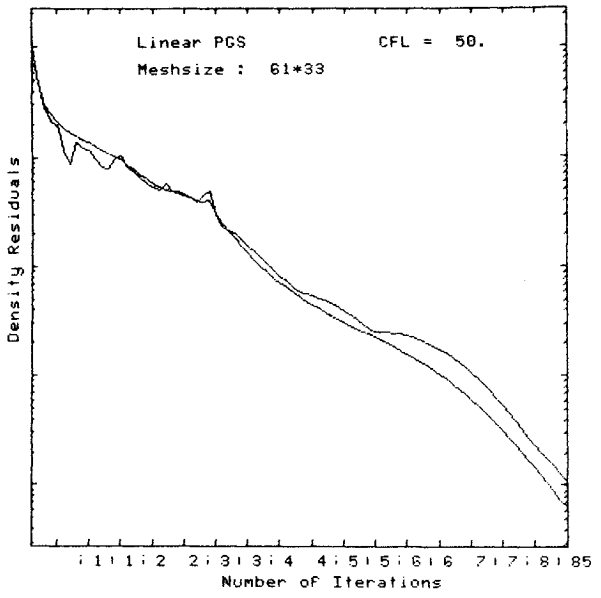

Fig. 3 Convergence history channel with wedges for the monotone characteristic scheme.

Both schemes were tested for an oblique shock-reflection problem, and the results were compared with those obtained with classical upwind methods.

The following observations were made: 1) the shock resolution obtained with the classical first-order upwind scheme was not improved as compared to first-order accurate flux vector splitting; and 2) the streamline upwind scheme, although only first-order accurate, leads to a shock resolution comparable to the one obtained with classical second-order accurate schemes.

This leads to the following conclusions: in order to fully exploit the possibilities of this approach it is not sufficient to detect the characteristic directions, but a suitable algorithm must be used to discretize the resulting convection equations.

In the following sections, conservative schemes based on the characteristic approach will be discussed.

Conservative Solution Algorithm

In the present section, a conservative scheme will be defined using numerical fluxes based on the characteristic directions and variables. More details can be found in Ref. 14. Conservativity is ensured by using Roe averages in the expressions for the matrices P^{*-1} and P^*.

A first-order upwind scheme for Eq. (9) is given by

$$
\begin{aligned}
U_{ij}^{n+1} - U_{ij}^{n} = &- \frac{\Delta t}{2\Delta x} \sum_l R^l_{i-1/2,j} \underline{[\Lambda^l_x} \\
&+ |\Lambda^l_x|]_{i-1/2,j} \underline{[w^l_{ij} - w^l_{i-1,j}]} \\
&- \frac{\Delta t}{2\Delta x} \sum_l R^l_{i+1/2,j} \underline{[\Lambda^l_x} \\
&- |\Lambda^l_x|]_{i+1/2,j} \underline{[w^l_{i+1,j} - w^l_{i,j}]} \\
&- \frac{\Delta t}{2\Delta x} \sum_l R^l_{i-1/2,j} \sum_k (c^{lk}_x)_{i-1/2,j} [w^k_{ij} - w^k_{i-1,j}] \\
&- \frac{\Delta t}{2\Delta x} \sum_l R^l_{i+1/2,j} \sum_k (c^{lk}_x)_{i+1/2,j} [w^k_{i+1,j} - w^k_{ij}] \\
&- \text{similar terms in } y \text{ direction} \qquad (16)
\end{aligned}
$$

The $c^{lk}_{x(y)}$ in Eq. (16) stands for component l,k of the matrix $C_{x(y)}$. Note that these coupling terms are discretized centrally. The vectors R^l in Eq. (16) are the columns of the matrix P^* of Eq. (7) and Δw^l the lth component of the discretization of vector ∂W; cf. Eq. (8). The vectors R^l and the eigenvalues Λ^l_x, Λ^l_y are evaluated at the cell faces, from the expressions given, respectively, in Eqs. (7) and (12).

This requires the knowledge of the characteristic directions and the conservative variables at each cell face. The characteristic directions are obtained from the local gradients of pressure and velocity components; cf. Eqs. (14) and (15). These gradients are calculated at the two corners of the cell face. At each corner the gradient is obtained by integrating over the surrounding dual cell; i.e., a cell with cell centers as corner nodes, according to

$$\nabla\phi = \frac{1}{\Omega}\int_\Omega \nabla\phi \mathrm{d}\Omega = \frac{1}{\Omega}\oint_s \phi \boldsymbol{n} \mathrm{d}S \qquad (17)$$

The conservative variables on the cell face are obtained by averaging the values available at the cell centers on both sides of the face. Instead of arithmetic averages, Roe averages are used; cf. Ref. 11.

As a result, the underlined terms of Eq. (16) and similar ones in the y direction can further be worked out, using Eq. (10) and (11). By doing so the coupling terms of Eq. (16) cancel out. The resulting scheme can be written in flux form with the following definition of the numerical flux:

$$
\begin{aligned}
F_{i+1/2,j} &= \tfrac{1}{2}(F_{ij} + F_{i+1,j}) \\
&- \tfrac{1}{2}\sum_l R^l_{i+1/2,j} |\Lambda^l_x|_{i+1/2,j} [w^l_{i+1,j} - w^l_{i,j}] \qquad (18)
\end{aligned}
$$

and a similar relation for the numerical flux in the y direction.

As already mentioned in the Introduction, the expression for the numerical flux is very similar to that used in flux-difference splitting.[11] However, the eigenvectors R^l, the eigenvalues Λ^l, and the variables w^l are now functions of the characteristic directions instead of the grid directions.

Since the coupling terms do not appear in Eq. (18), it can be used for each possible choice of the directions $\boldsymbol{\kappa}_1$, $\boldsymbol{\kappa}_2$. If for instance one chooses both characteristic directions equal to the cell normal, Roe's flux-differencing scheme is recovered. However, only the choice according to Eq. (14) and

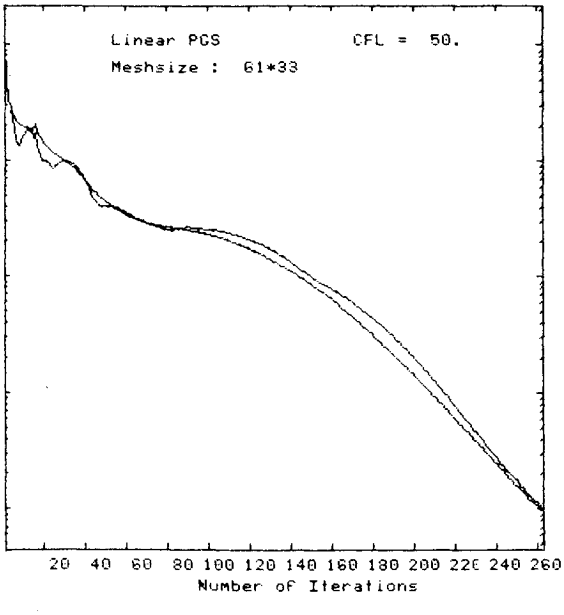

Fig. 4 Convergence history channel with wedges for the nonmonotone characteristic scheme.

(15) allows to mimic more closely the physics of the flow and may reduce the numerical mesh dependency.

Note that the characteristic variables are only determined up to a scaling factor. The choice of this scaling factor may have some impact on the stability of the numerical scheme. Within the framework of hypersonic flows and total variation diminishing schemes, Yee[15] suggests scaling of the characteristic variables so that their variations are of the same order of magnitude as the pressure differences. In the present context, the definition of Eq. (8) was used in all test cases. No numerical problems resulting from this particular choice were encountered. It should be noted however that none of the problems dealt with hypersonic flow.

The scheme is easily extended to nonCartesian grids. The numerical flux is given by

$$(\boldsymbol{F}\cdot\boldsymbol{n})_{i+1/2,j} = \tfrac{1}{2}(\boldsymbol{F}_{ij} + \boldsymbol{F}_{i+1,j})\cdot\boldsymbol{n}_{i+1/2,j} - \tfrac{1}{2}\sum_l R^l_{i+1/2,j}\,|\boldsymbol{\Lambda}^l\cdot\boldsymbol{n}|_{i+1/2,j}\,[w^l_{i+1,j} - w^l_{i,j}] \tag{19}$$

with $\boldsymbol{n}$ the outward pointing unity normal on the cell faces and

$$\boldsymbol{\Lambda}^l = (\Lambda^l_x, \Lambda^l_y) \tag{20}$$

The conservative scheme described above is only first-order accurate in space. It has been derived based on the classical upwind scheme; cf. Eq. (16). Referring to the conclusions of the previous section, no improvement in accuracy as compared to the classical schemes is to be expected. This was confirmed in several test cases.

The present scheme can easily be extended to higher-order accuracy using a classical MUSCL extrapolation. The resulting scheme has an improved resolution but the accuracy is comparable to that obtained with classical higher-order methods.

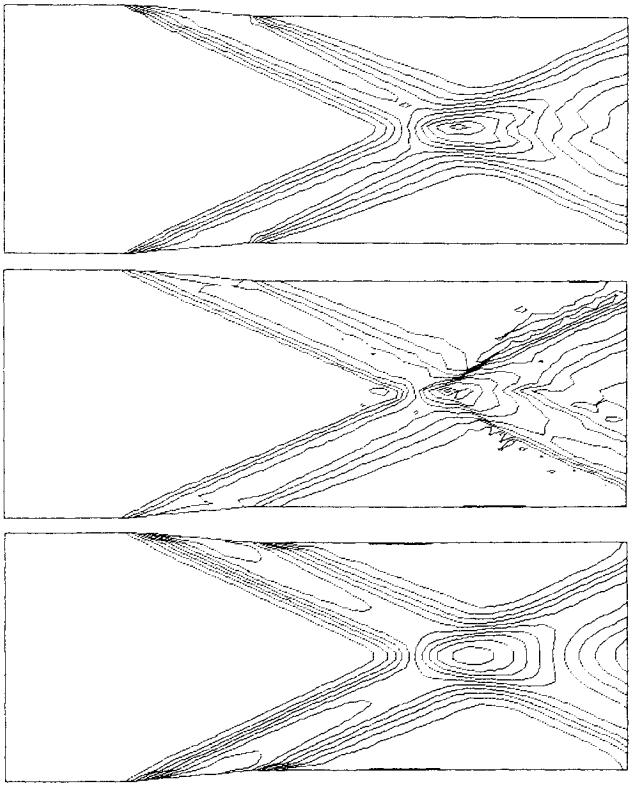

Fig. 5 Iso-Mach lines for the flow in the channel with wedges: a) monotone characteristic; b) nonmonotone characteristic; and c) second-order van Leer flux vector splitting.

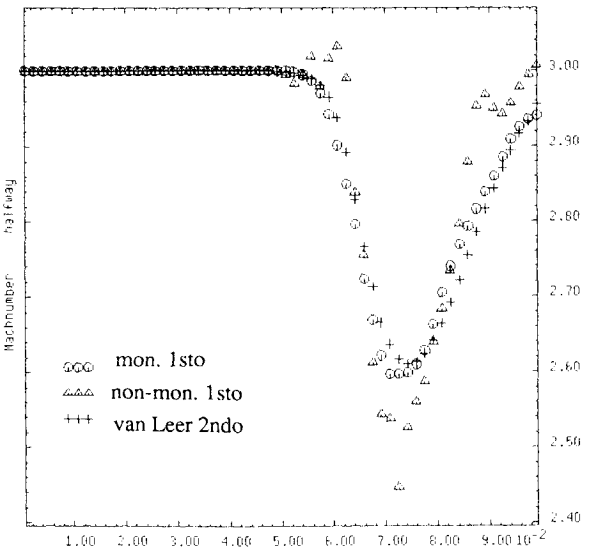

Fig. 6 Mach number distribution along streamwise direction, halfway the channel with wedges.

Since within the present approach the real directions of information propagation are known, the classical MUSCL extrapolation may be replaced by a MUSCL extrapolation into the characteristic directions. This "characteristic MUSCL extrapolation" may be used to extend the spatial accuracy of the scheme to second order: this requires a first-order extrapolation. However, one can also use a zero-order characteristic extrapolation; the spatial accuracy of the resulting scheme is then still of first order, but with a reduced cross diffusion.

The characteristic MUSCL approach is discussed in the next section.

Characteristic MUSCL Extrapolation

The idea is first worked out for the following linear, scalar, convection equation:

$$\frac{\partial w}{\partial t} + \frac{\partial (aw)}{\partial x} + \frac{\partial (bw)}{\partial y} = 0 \tag{21}$$

In the present approach, it is assumed that the time discretization and the spatial discretization are uncoupled. In the following, the spatial discretization is discussed, and the treatment of the time derivative is left unspecified. Equation (21) can be discretized in space as follows:

$$\begin{aligned}\frac{\partial w}{\partial t}\Delta t &+ \tfrac{1}{2}(\sigma_x - |\sigma_x|)\,(w^-_{i+1/2,j} - w^-_{i-1/2,j}) \\ &+ \tfrac{1}{2}(\sigma_x + |\sigma_x|)\,(w^+_{i+1/2,j} - w^+_{i-1/2,j}) \\ &+ \tfrac{1}{2}(\sigma_y - |\sigma_y|)\,(w^-_{i,j+1/2} - w^-_{i,j-1/2}) \\ &+ \tfrac{1}{2}(\sigma_y + |\sigma_y|)\,(w^+_{i,j+1/2} - w^+_{i,j-1/2})\end{aligned} \tag{22}$$

where σ_x, σ_y are the CFL numbers in the x and y directions, respectively. The $w^-_{i\pm 1/2,j}$, $w^+_{i\pm 1/2,j}$ are values on the cell faces $i \pm 1/2, j$ obtained by a suitable extrapolation, biased into the downwind (i.e., positive) and the upwind (i.e., negative) x direction, respectively. Similarly, the values $w^-_{i,j\pm 1/2}$, $w^+_{i,j\pm 1/2}$ are found by an extrapolation biased into the downwind and the upwind y direction.

The simplest choice corresponds to a zero-order extrapolation:

$$w^-_{i+1/2,j} = w_{i+1,j} \qquad w^+_{i+1/2,j} = w_{i,j} \tag{23}$$

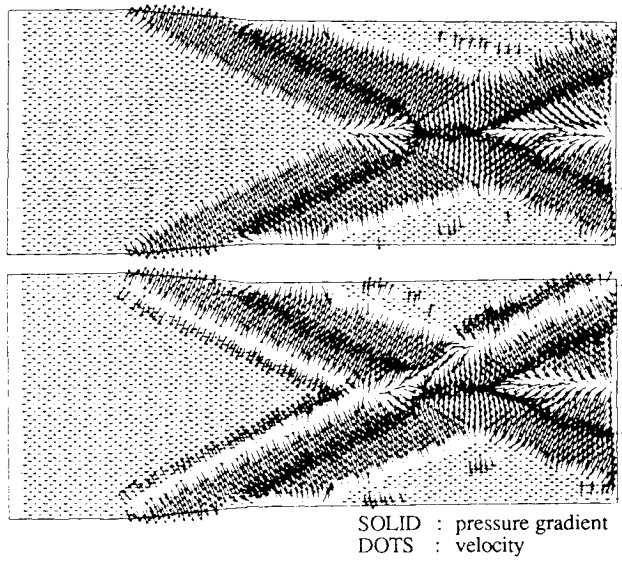

Fig. 7 κ_1 directions for the channel with wedges: a) monotone characteristic; b) nonmonotone characteristic.

and similar relations for the values of the remaining cell faces. For this choice, the scheme (22) reduces to the classical first-order upwind scheme.

A higher-order scheme results if a first-order extrapolation is used. In the classical MUSCL extrapolation, the mesh directions are used to extrapolate the variables to the cell faces.

Instead, one might consider to extrapolate along the convection direction. This approach will be referred to as characteristic MUSCL extrapolation.

If one restricts the extrapolation to the first cell centers nearest to the cell face, the extrapolation is of zero-order along the characteristic direction, resulting in a first-order accurate scheme. Referring to Fig. 1, one obtains

$$w^-_{i+1/2,j} = w_P \qquad w^+_{i+1/2,j} = w_M \tag{24}$$

The values w_M and w_P are obtained by linear extrapolation between nodes $i,j/i,j-1$ and $i+1,j/i+1,j+1$, respectively. Similarly, on cell face $i,j+\frac{1}{2}$ one has

$$w^-_{i,j+1/2} = w_T \qquad w^+_{i,j+1/2} = w_R \tag{25}$$

The same procedure is applied for the remaining cell sides. If σ_x and σ_y are positive and satisfy

$$\frac{1}{2} \le \frac{\sigma_y}{\sigma_x} \le 2 \tag{26}$$

the following scheme results

$$\frac{\partial w}{\partial t}\Delta t + \frac{1}{2}(\sigma_x + \sigma_y)w_{i,j} + \frac{1}{2}(\sigma_x - \sigma_y)w_{i,j-1} + \frac{1}{2}(-\sigma_x + \sigma_y)w_{i-1,j} - \frac{1}{2}(\sigma_x + \sigma_y)w_{i-1,j-1} = 0 \tag{27}$$

This scheme is due to Raithby[16] who developed it within the context of convection-diffusion problems. If the first unequality is not satisfied, points R,T lie outside the intervals $[i-1,j;\ i,j]$ and $[i,j+1;\ i+1,j+1]$. In this case, the values w_R, w_T will be clipped and put equal to $w_{i-1,j}$ and $w_{i+1,j+1}$, respectively. Similarly, if the second unequality is not satisfied, the values w_M, w_T are put equal to $w_{i,j-1}$ and $w_{i+1,j+1}$. Although this scheme is only first-order accurate in space, it is not monotone. Its numerical diffusion however is considerably less than for the classical first-order upwind scheme.[17]

Also note that this scheme gives the exact solution for a flow angle of 45 deg.

A simplified version results if, instead of interpolating between nodes i,j and $i,j-1$, one assigns the value $w_{i,j}$ to w_M if M lies closer to node i,j than to node $i,j-1$ and $w_{i,j-1}$ if not. The same procedure is applied for w_P and the intersections resulting from the remaining cell sides. The resulting scheme is

$$\frac{\partial w}{\partial t}\Delta t + \sigma_x[w_{i,j} - w_{i-1,j}] + \sigma_y[w_{i-1,j} - w_{i-1,j-1}] = 0, \qquad \sigma_x > \sigma_y \tag{28a}$$

$$\frac{\partial w}{\partial t}\Delta t + \sigma_x[w_{i,j-1} - w_{i-1,j-1}] + \sigma_y[w_{i,j} - w_{i,j-1}] = 0, \qquad \sigma_x < \sigma_y \tag{28b}$$

This corresponds to the streamline upwind scheme derived from Ref. 13 and mentioned previously. It is only first-order accurate and monotone. It is also less diffusive than the classical first-order upwind scheme[17] and gives the exact solution for a flow angle of 45 deg.

To extend the characteristic MUSCL extrapolation to higher-order accuracy, more nodes must be involved in the determination of $w_{i\pm1/2,j}$ and $w_{i,j\pm1/2}$.

Referring to Fig. 1, one possibility is to use the nodes M and N to determine $w^-_{i+1/2,j}$ and P,Q for $w^+_{i+1/2,j}$. One finds

$$w^+_{i+1/2,j} = \frac{3}{2}\left[1 - \frac{\sigma_y}{2\sigma_x}\right]w_{i,j} + \frac{3}{4}\frac{\sigma_y}{\sigma_x}w_{i,j-1} - \frac{\sigma_y}{4\sigma_x}w_{i-1,j-2} - \frac{1}{2}\left[1 - \frac{\sigma_y}{2\sigma_x}\right]w_{i-1,j-1} \tag{29a}$$

$$w^-_{i+1/2,j} = \frac{3}{2}\left[1 - \frac{\sigma_y}{2\sigma_x}\right]w_{i+1,j} + \frac{3}{4}\frac{\sigma_y}{\sigma_x}w_{i+1,j+1} - \frac{\sigma_y}{4\sigma_x}w_{i+2,j+2} - \frac{1}{2}\left[1 - \frac{\sigma_y}{2\sigma_x}\right]w_{i+2,j+1} \tag{29b}$$

Similarly, the intersections R,S and T,U are used to determine $w^+_{i,j+1/2}$ and $w^-_{i,j+1/2}$, respectively. Assuming that the convection is into the positive x and y directions and that

$$\frac{3}{4} \le \frac{\sigma_y}{\sigma_x} \le \frac{4}{3} \tag{30}$$

the steady-state molecule of Fig. 2 is obtained.

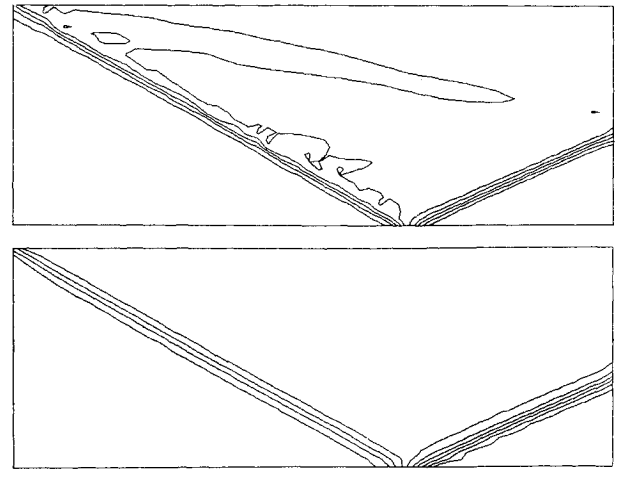

Fig. 8 Density isolines for the oblique shock flow: a) monotone characteristic. b) second-order van Leer flux vector splitting.

If condition (30) is not satisfied, some of the nodes M, N, P, Q or R, S, T, U will be clipped and the scheme becomes locally first-order accurate.

The stability of this scheme as well as that of the first-order accurate schemes (27) and (28) was investigated using a von Neumann analysis, for different flow angles. Only Euler-implicit time integration was considered.

It is found that, although all of the schemes are stable, only scheme (28) is a good "smoother." The other schemes do not damp the high-frequency modes $(\theta_x,\theta_y) = (\pm\pi,\pm\pi)$. It can be shown that this property is valid for all schemes with an antisymmetric (steady-state) molecule across the diagonal $i = j$. The Fourier footprint ϕ(Res) of such a molecule equals 0 for any of the combinations $\theta_x = \pm\pi$, $\theta_y = \pm\pi$. Hence, the amplification factor which is given by

$$\zeta = 1 - \phi(\text{Res}) \tag{31}$$

for the explicit scheme and

$$\zeta = [1 + \phi(\text{Res})]^{-1} \tag{32}$$

for the implicit scheme, becomes unity.

Genuinely Multidimensional Euler Schemes

Genuinely multidimensional schemes for the Euler equations are obtained by combining the conservative, first-order accurate scheme of Eq. (19), with the characteristic MUSCL extrapolation described in the previous section.

The numerical flux vector Eq. (19) is rewritten as

$$(\boldsymbol{F}\cdot\boldsymbol{n})_{i+1/2,j} = \frac{1}{2}(\boldsymbol{F}^{+}_{i+1/2,j} + \boldsymbol{F}^{-}_{i+1/2,j})\cdot\boldsymbol{n}_{i+1/2,j} - \frac{1}{2}\sum_{l} R^{l}_{i+1/2,j}\,|\boldsymbol{\Lambda}^{l}\cdot\boldsymbol{n}|_{i+1/2,j}\,[w^{l-}_{i+1/2,j} - w^{l+}_{i+1/2,j}] \tag{33}$$

where the superscripts plus and minus indicate upwind and downwind extrapolations with respect to the direction of the normal $\boldsymbol{n}$. The first two terms in the right-hand side of Eq. (33) are calculated as follows:

$$(\boldsymbol{F}^{\pm}\cdot\boldsymbol{n})_{i+1/2,j} = \boldsymbol{F}\cdot\boldsymbol{n}(U^{\pm}_{i+1/2,j}) \tag{34}$$

with

$$U^{+}_{i+1/2,j} = U_{i,j} + P^{*}(W^{+}_{i+1/2,j} - W_{i,j}) \tag{35a}$$

$$U^{-}_{i+1/2,j} = U_{i+1,j} + P^{*}(W_{i+1/2,j} - W_{i+1,j}) \tag{35b}$$

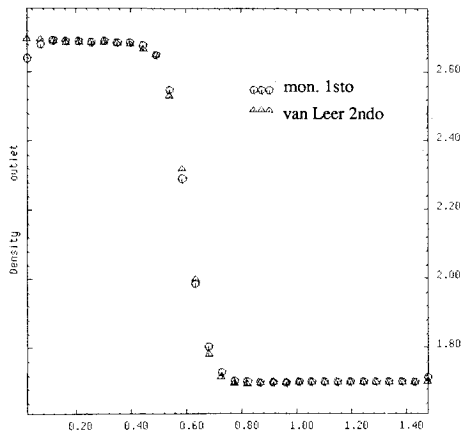

Fig. 9 Density distribution for the oblique shock flow at the outlet section.

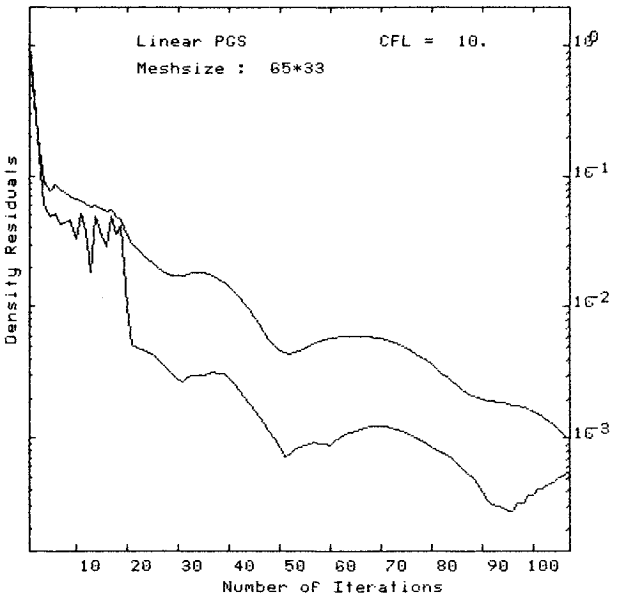

Fig. 10 Convergence history channel with bump for the monotone characteristic scheme.

The variations of the characteristic variables in Eqs. (33) and (35) are obtained using the characteristic MUSCL extrapolation. For component l of W, the extrapolation is into the corresponding characteristic propagation direction $\boldsymbol{\Lambda}^{l}$. One has

$$\boldsymbol{\Lambda}^{1} = \boldsymbol{\Lambda}^{2} = \boldsymbol{v} \qquad \boldsymbol{\Lambda}^{3} = \boldsymbol{v} + c\cdot\boldsymbol{\kappa}_2 \qquad \boldsymbol{\Lambda}^{4} = \boldsymbol{v} - c\cdot\boldsymbol{\kappa}_2 \tag{36}$$

Referring to Fig. 1;

$$w^{+}_{i+1/2,j} = w_M + \left|\frac{AM}{MN}\right|(w_M - w_N) \tag{37}$$

where the superscript l, denoting the component of the vector of characteristic variables, is dropped for clarity. A similar formula is used for $w^{-}_{i+1/2,j}$ involving points P and Q. Expressing w_M, w_N, w_P, w_Q as a linear combination of the values in the nodes of the respective cell faces, one obtains

$$w^{+}_{i+1/2,j} - w_{i,j} = \alpha_1(w_{i,j} - w_{i,j-1}) + \alpha_2(w_{i,j-1} - w_{i-1,j-1}) + \alpha_3(w_{i-1,j-1} - w_{i-1,j-2}) \tag{38}$$

and

$$w^{-}_{i+1/2,j} - w_{i+1,j} = \beta_1(w_{i+1,j+1} - w_{i+1,j}) + \beta_2(w_{i+2,j+1} - w_{i+1,j+1}) + \beta_3(w_{i+2,j+2} - w_{i+2,j+1}) \tag{39}$$

where the coefficients α,β depend on the mesh geometry and the characteristic propagation direction. For the first-order schemes, one has

$$\alpha_2 = \alpha_3 = 0 \qquad \beta_2 = \beta_3 = 0 \tag{40}$$

It is easily verified that this approach reduces to the schemes derived in the previous section for a scalar, linear convection equation.

The present scheme requires no special treatment of the boundary conditions: identical boundary conditions can be used as for the flux vector splitting code.

To ensure fast convergence toward steady state, and to allow for high CFL numbers, the present scheme is combined

with an implicit time discretization. The chosen implicit operator is that of van Leer flux vector splitting. Although it has been found that an inconsistency between implicit and explicit operators may lead to convergence problems,[18] no convergence problems of this type were encountered in the present applications.

Results

In the present paper, only results for the first-order accurate schemes will be shown. Three test cases are considered: the supersonic flow through a channel with 5-deg wedges on lower and upper wall, an oblique shock reflection problem, and the subsonic flow through a channel with a 10% bump on the lower wall.

Test Case 1

The first test case is the supersonic flow through a channel with 5-deg wedges on lower and upper wall; cf. Ref. 19. The inlet Mach number equals 3. The mesh used in the present calculations consists of 60 × 32 cells.

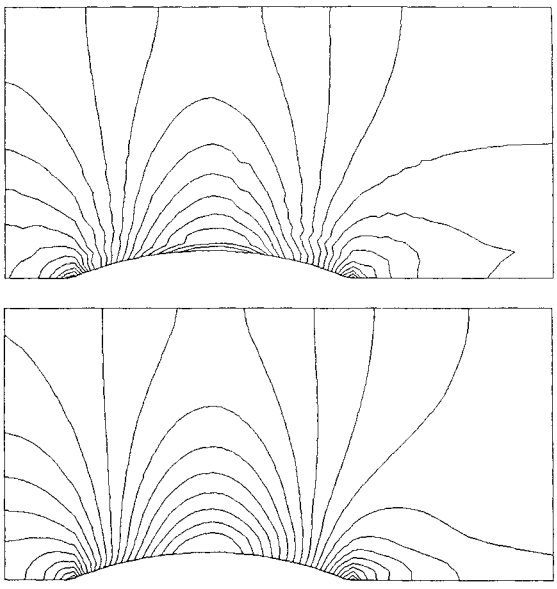

Fig. 11 Iso-Mach lines for the flow in the channel with bump: a) monotone characteristic; b) second-order van Leer flux vector splitting.

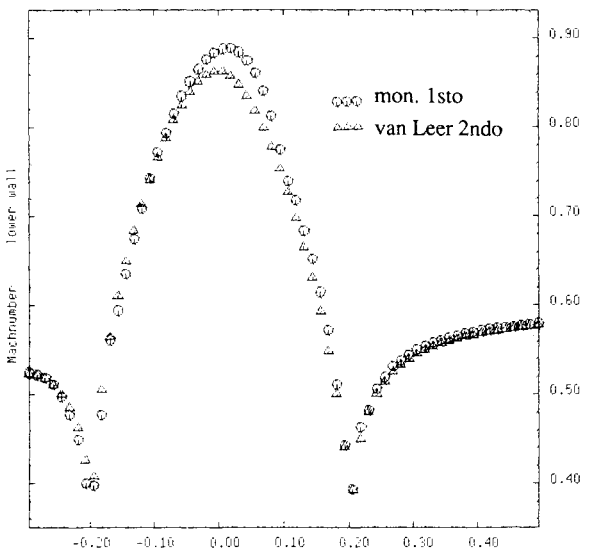

Fig. 12 Mach number distribution along the lower wall for the channel with bump.

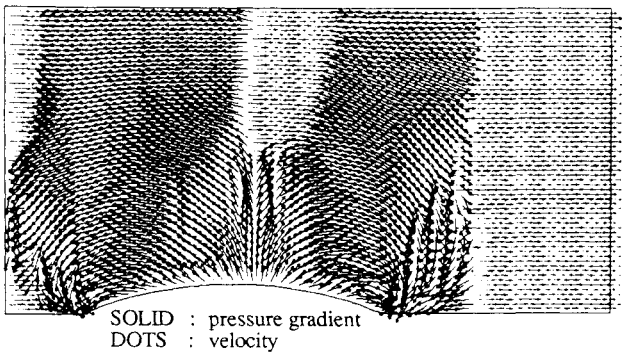

Fig. 13 κ_1 directions for the channel with bump for the monotone characteristic scheme.

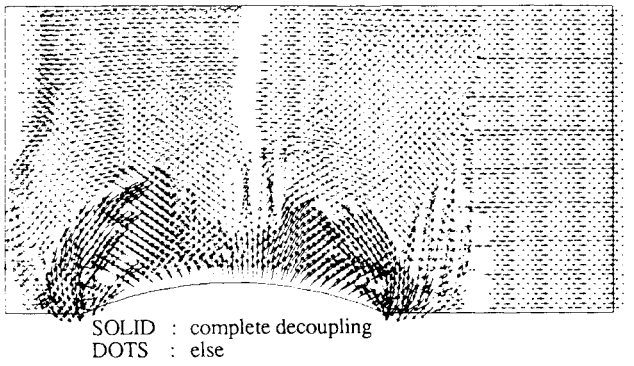

Fig. 14 κ_2 directions for the channel with bump for the monotone characteristic scheme.

Calculations were performed with two versions of the first-order characteristic MUSCL scheme: the monotone version, cf. Eq. (28) and the nonmonotone version, cf. Eq. (27). The results are compared with a second-order accurate van Leer flux vector splitting solution on the same mesh. The minmod limiter was used to ensure monotonicity for the second-order accurate solution.

Figures 3 and 4 show the convergence history of the monotone and the nonmonotone characteristic scheme, respectively. The monotone characteristic scheme converges in approximately the same number of iterations as the flux vector splitting scheme (not shown). Comparison of Figs. 3 and 4 shows that the nonmonotone characteristic scheme requires about three times as many iterations. The reason is the poor damping of the high-frequency errors, as indicated by the von Neumann analysis.

It is also to be noted that, in order to obtain convergence for the characteristic calculations, the characteristic normals were frozen after a residual drop of about 10^{-1}. If they are recalculated every iteration, the convergence ends in a limit cycle as a result of the numerical noise on the detection of these directions.

Figure 5 compares the calculated iso-Mach lines for the three schemes. It is clear that the resolution of the shocks and of the expansion fan obtained with the present first-order accurate schemes is at least as good as that obtained with the second-order accurate flux vector splitting scheme.

The present computations were performed in the complete configuration: no symmetry condition was used. This results in a nonsymmetric solution for the characteristic schemes due to the asymmetry of the calculated characteristic normals.

Figure 6 compares the streamwise Mach number distribution halfway the channel. It illustrates the nonmonotonicity of the characteristic scheme based on Eq. (27). It also shows that the latter scheme captures the shock slightly sharper than the other schemes.

Figure 7 shows the calculated κ_1 directions for the two characteristic schemes. In the nonuniform flow regions, near shocks and expansion fans, κ_1 is directed along the pressure gradients. In the regions of small pressure gradients, κ_1 is taken into the flow direction. Note that in this calculation no blending of the pressure gradient direction and the flow direction was used.

The κ_2 directions are not shown since they coincide with the κ_1 directions in the present calculations. This is because the velocity gradients were considered too small (less than 1% of the velocity modulus scaled by the cell area), in order to solve Eq. (15). In this case one chooses $\kappa_2 = \kappa_1$.

Test Case 2

The second test case is the reflection of an oblique shock along a flat plate. Calculations were performed with the monotone first-order characteristic scheme and second-order van Leer flux vector splitting (with minmod limiting) for comparison.

The channel is discretized with 61 × 33 mesh points. At inlet, the Mach number is 2.9 and the flow is purely axial. Along the upper boundary, all of the dependent variables are imposed. On the lower wall the velocity is tangential and the pressure is extrapolated from the interior. At outlet, all of the dependent variables are extrapolated.

Figure 8 shows the density isolines for the two schemes. The shocks of the present first-order accurate scheme are slightly sharper than those of the second-order accurate van Leer scheme. The present solution shows some "noise" behind the impingent shock. This is due to the switching of the κ_1 direction, as explained above, and may be removed by blending the pressure gradient direction and the flow direction.

Figure 9 shows the density distribution along the outlet section.

Test Case 3

This test case deals with a fully subsonic flow in a channel with a 10% bump on the lower wall. The inlet Mach number is 0.6. Again results obtained with the monotone characteristic scheme and van Leer flux vector splitting are compared. The computations were performed on a 65 × 33 mesh.

Figure 10 shows the convergence history of the present scheme. The characteristic directions were frozen after 20 iterations. The convergence rate is similar to that of flux vector splitting (not shown).

Figure 11 shows the computed iso-Mach lines. The solutions obtained with both schemes are qualitatively in good agreement. The present solution however is less "smooth" than the one obtained with flux vector splitting. This can be attributed to the switching in characteristic directions, and will be removed using blending.

In Fig. 12, the Mach number distribution along the lower wall is shown. Although the overall agreement is good, there is some difference in the value of the maximum Mach number. It is not clear whether this is caused by the difference in spatial accuracy of both schemes. This should be confirmed in calculations with the second-order accurate characteristic scheme.

Finally, Figs. 13 and 14 show the characteristic directions. It can be observed that in this application there is a large zone, near the bump, where both Eqs. (14) and (15) are solved, and hence a complete diagonalization of the Euler system is obtained.

Conclusions

New upwind, multidimensional Euler schemes have been formulated based on numerical fluxes depending on characteristic directions that diagonalize the Euler system. The mesh dependency of the scheme is further reduced using a MUSCL extrapolation into these directions. This leads to the definition of new first- and second-order accurate schemes.

In the present paper, the first-order accurate version was tested. The results indicate that this scheme resolves strong flow gradients as accurate as classical higher-order schemes. They are, however, sensitive to the accuracy of the determination of the characteristic directions. This requires further investigation in order to improve the robustness of the schemes.

References

[1]Steger J. L., and Warming, R. F., "Flux Vector Splitting of the Inviscid Gas Dynamic Equations with Applications to Finite-Difference Methods," *Journal of Computational Physics*, Vol. 40, 1981, pp. 263–293.

[2]van Leer B., "Flux Vector Splitting for the Euler Equations," *Lecture Notes in Physics*, Vol. 170, Springer-Verlag, Berlin, 1982, pp. 507–512.

[3]Godunov, S. K., "A Difference Method for the Numerical Computation of Discontinuous Solutions of Hydrodynamic Equations," *Math Sbornik*, Vol. 47, 1959, pp. 271–306. (Translated as JPRS 7225 by U.S. Dept. of Commerce, 1960.)

[4]Roe, P. L., "The Use of the Riemann Problem in Finite-Difference Schemes," *Proceedings of the 7th International Conference on Numerical Methods in Fluid Dynamics*, Lecture Notes in Physics, Vol. 141, Springer-Verlag, 1981, pp. 354–359.

[5]Osher, S., and Solomon, F., "Upwind Schemes for Hyperbolic Systems of Conservations Laws," *Mathematics of Computation*, Vol. 38, No. 158, 1982, pp. 339–377.

[6]Roe, P. L., "Discrete Models for the Numerical Analysis of Time-Dependent Multidimensional Gas Dynamics," *Journal of Computational Physics*, Vol. 63, No. 2, 1986, pp. 458–476.

[7]Hirsch, Ch., "A Diagonalization Approach for the Multidimensional Euler Equations," *Proceedings of the 4th Seminar on High-Speed Aerodynamics*, edited by A. Nastase, 1985.

[8]Deconinck, H., Hirsch, Ch., and Peuteman, J., "Characteristic Decomposition Methods for the Multidimensional Euler Equations," 10th International Conf. on Numerical Methods in Fluid Dynamics, Beijing, June 1986.

[9]Hirsch, Ch., Lacor, C., and Deconinck, H., "Convection Algorithms Based on a Diagonalisation Procedure for the Multidimensional Euler Equations," AIAA Paper 87-1163, June 1987.

[10]Powell, K. G., and van Leer, B., "A Genuinely Multidimensional Upwind Cell-Vertex Scheme for the Euler Equations, AIAA Paper 89-0095, June 1989.

[11]Roe, P. L., "Approximate Riemann Solvers, Parameter Vectors, and Difference Schemes, *Journal of Computational Physics*, Vol. 43, 1981, pp. 357–382.

[12]Levy, D. W., Powell, K. G., and van Leer, B., "An Implementation of a Grid-Independent Upwind Scheme for the Euler Equations," AIAA Paper 89-1931, 1989.

[13]Rice, J. G., Schnipke, R. J., "A Monotone Streamline Upwind Finite Element for Convection Dominated Flows," *Computer Methods in Applied Mechanics and Engineering*, Vol. 48, 1985, pp. 313–327.

[14]Hirsch, Ch., and Lacor, C., "Upwind Algorithms Based on a Diagonalization of the Multidimensional Euler Equations," AIAA Paper 89-1958, June 1989.

[15]Yee, H. C., "A Class of High-Resolution Explicit and Implicit Shock-Capturing Methods," *Von Kármán Institute Lecture Series*, LS 89-04, 1989.

[16]Raithby, G. D., "Skew Upstream Differencing Schemes for Problems Involving Fluid Flow," *Computer Methods in Applied Mechanics and Engineering*, Vol. 9, 1976, pp. 153–164.

[17]Lacor, C., "A Computational Method for Steady, Three-Dimensional, Inviscid, Subsonic Flows," Ph.D. Thesis, Vrije Universiteit Brussel, Brussels, Belgium, 1985–1986.

[18]Liou, M. S., and van Leer, B., "Choice of Implicit and Explicit Operators for the Upwind Differencing Method," AIAA Paper 88-0624, Jan. 1988.

[19]Walters, R. W., and Dwoyer, D. L., "An Efficient Iteration Strategy for the Solution of the Euler Equations," AIAA Paper 85-1529, 1985.